УДК 621.793.18

SYNTHESIS, STRUCTURE AND OPTICAL PROPERTIES OF TiO_2 AND TiO_2/Al_2O_3 THIN FILMS DEPOSITED ON INDIUM TIN OXIDE SUBSTRATES PREPARED BY CHEMICAL BATH DEPOSITION

SAMEERAH S. S. AL-QADASY[1], S. Q. CHISHTY[1], HAKIM Q. N. M. AL-ARIQUE[2], SAMI M. A. AL-ARIKI[3], NIYAZI A. S. AL-AREQI[2]

[1]Department of Physics, Dr. Rafiq Zakaria College for Women, Aurangabad University, the Republic of India

[2]Department of Chemistry, Taiz University, the Republic of Yemen

[3]Department of Physics, Thamar University, the Republic of Yemen

TiO_2 and TiO_2/Al_2O_3 thin films were applied on glass substrates containing indium and tin oxides (ITO) from a solution containing $Ti[OCH(CH_3)_2]4$ and $AlCl_3 \cdot 6H_2O$ at room temperature using a simple and economical method of chemical bath deposition (CBD-method). Then, the obtained thin films were annealed at 500 °C for two hours. The structural, morphological and optical properties of TiO_2 and TiO_2/Al_2O_3 thin films were analyzed by X-ray diffraction (XRD), field emission scanning electron microscopy (FE-SEM), Fourier-transform infrared spectroscopy (FT-IR), Raman spectroscopy and UV-visible spectrophotometry. The XRD results showed that the average size of TiO2 crystallites is 58.6 and 22.8 nm before and after annealing, whilst the average size of TiO_2/Al_2O_3 before annealing is 56 nm with the anatase phase and then after annealing crystallites with tetragonal symmetry are formed with a size of ~ 17 nm. The anatase peaks appeared at an annealing temperature of 500 °C indicating an increase in crystallinity during the annealing process. However, FT-IR analysis showed the presence of absorption peaks for various functional groups, such as O–H, CH, Ti–O–Ti, Al–O). The appearance of the anatase peak at 144 cm^{-1} and sharp clear peaks after annealing also indicates an increase in crystallinity. FE-SEM images revealed an elongated spherical shape for TiO 2 nanocrystals and a nanoplatelet shape for TiO2/Al2O3. The optical band gap width for TiO2 thin films was 3.28 and 3.07 eV before and after annealing and for TiO_2/Al_2O_3 thin films it decreased from 3.32 to 3.14 eV after annealing.

Keywords: thin films, TiO_2/Al_2O_3, CBD-method, annealing, optical band gap width.

СИНТЕЗ, СТРУКТУРА И ОПТИЧЕСКИЕ СВОЙСТВА ТОНКИХ ПЛЕНОК TiO_2 И TiO_2/Al_2O_3, НАНЕСЕННЫХ НА ПОДЛОЖКИ ИЗ ОКСИДА ИНДИЯ И ОЛОВА, ПРИГОТОВЛЕННЫЕ МЕТОДОМ ХИМИЧЕСКОГО ОСАЖДЕНИЯ В ВАННЕ

САМЕЕРА С. С. АЛЬ-КАДАСИ[1], С. К. ЧИШТИ[1], ХАКИМ К. Н. М. АЛЬ-АРИКИ[2], САМИ М. А. АЛЬ-АРИКИ[3], НИВАЗИ А. С. АЛЬ-АРИКИ[2]

[1]Кафедра физики Рафия Закария женского колледжа, Аурангабадский университет, Республика Индия

[2]Кафедра химии, Таизский университет, Республика Йемен

[3]Кафедра физики, Дамарский университет, Республика Йемен

Тонкие пленки TiO_2 и TiO_2/Al_2O_3 осаждались на стеклянных подложках содержащих оксиды индия и олова (ITO) из раствора, содержащего $Ti[OCH(CH_3)_2]_4$ и $AlCl_3 \cdot 6H_2O$ при комнатной температуре с использованием простого и экономичного метода химического осаждения в ванне (CBD-метод). Затем по-

лученные тонкие пленки отжигали при 500 °C в течение двух часов. Структурные, морфологические и оптические свойства тонких пленок TiO_2 и TiO_2/Al_2O_3 исследовались методами рентгеновской дифракции (XRD), полевой эмиссионной сканирующей электронной микроскопией (FE-SEM), инфракрасной Фурье-спектрометрией (FT-IR), спектроскопией комбинационного рассеяния и УФ-видимой спектрофотометрией. Результаты XRD показали, что средний размер кристаллитов TiO_2 составляет 58,6 и 22,8 нм до и после отжига соответственно, тогда как средний размер TiO_2/Al_2O_3 до отжига составляет 56 нм с фазой анатаза, а затем после отжига формируются кристаллиты с тетрагональной симметрией с размером ~ 17 нм. Появление пиков анатаза при температуре отжига 500 °C указывает на увеличение кристалличности при отжиге. Однако FT-IR анализ показали присутствие пиков поглощения для различных функциональных групп, таких как O–H, CH, Ti–O–Ti, Al–O). Появление пика анатаза при 144 $см^{-1}$ и резких четких пиков после отжига также свидетельствует об усилении кристалличности. Изображения FE-SEM выявили удлиненную сферическую форму для нанокристаллов TiO_2 и форму нанопластинок для TiO_2/Al_2O_3. Ширина оптической запрещенной зоны для тонких пленок TiO_2 составила 3,28 и 3,07 эВ до и после отжига соответственно, а для тонких пленок TiO_2/Al_2O_3 после отжига уменьшилась с 3,32 до 3,14 эВ.

Ключевые слова: тонкие пленки, TiO_2/Al_2O_3, CBD-метод, отжиг, ширина оптической запрещенной зоны.

Introduction

Titanium dioxide (TiO_2) is a widely used material for photovoltaic and protective applications due to its high visible-region transparency, excellent mechanical properties and chemical stability in aqueous solution [1], [2]. TiO_2 films are also useful for many other applications such as catalysis [3], photonic coatings, gas sensors [4], and other electronic devices [5]. TiO_2 films have been prepared by a variety of chemical and physical deposition techniques, such as the sol-gel process [6]–[8], chemical vapor deposition [9], various reactive sputtering methods [10], [11], ion beam assisted processes [12], pulse laser deposition [13], chemical bath deposition [14], [15] atomic layer deposition [16] and evaporation [17]. It has been found that the physical properties of TiO_2 strongly depend on the deposition method applied and calcination temperatures. Generally, TiO_2 films change from amorphous to anatase and afterward to rutile based on the calcination temperature.

The dependences of structural and optical properties on annealing temperature have been reported [18]–[20]. The doping of TiO_2 with more foreign elements such as Zn, Mn, Fe, Ni, Al and Co affects TiO_2 nanoparticles. Its structural and optical properties allow it to be adapted for a variety of applications [21].

Al_2O_3 also known as alumina, is commercially produced from bauxite, an abundant ore, via the Bayer process. Al_2O_3 is similar to white powder (amorphous and polycrystals) or colorless hexagonal single crystals with a melting point about 2020 °C [22]. It is insoluble in water and organic liquids but very slightly soluble in acids and alkalis, it is a wonderful material that can show chemical resistance with good thermal stability.

Coating of materials such as thin films can impart these properties to protect other materials. Al_2O_3 it is widely used due to its high hardness, good chemical inertness, zero electrical conductivity and excellent optical transparency. A number of chemical and physical techniques have been reported for the fabrication of Al_2O_3 thin films [23]–[28]. Compared with conventional particles, nano-sized particles (e. g., iron, titanium, and alumina nanoparticles) definitely have a larger specific surface area which improves their super absorbent properties [29], [30]. So, in the present work, we have reported the successful utilization of the simple, cost-effective chemical bath deposition (CBD) method for preparation of nanocrystalline TiO_2 and TiO_2/Al_2O_3 thin films and studied the effect of annealing temperature on structural, morphological and optical properties of as- prepared thin films.

Experimental

Materials

Titanium isopropoxide Ti $[OCH(CH_3)_2]_4$ (TTIP), (98 %), purchased from Sigma-Aldrich Chemie, India was used as TiO_2 source. Aluminum chloride hexahydrate ($AlCl_3 \cdot 6H_2O$), (97 %), from Merck, Germany was used as Al_2O_3 source. Isopropanol

($CH_3CHOHCH_3$) (99 %) was obtained from Molychen. Mumbai, (India), and absolute ethanol (C_2H_5OH), (99.9 %) from Changshu Hongsheng Fine Chemical Co. Ltd., China. The conducting Indium tin oxide (ITO) coated glass (dimensions 75 mm × 25 mm × 1.1 mm, surface resistivity < 10 Ω/*sq*, was purchased from SHILP ENT and used as a substrate. Before the deposition, the substrates were cleaned by using chromic acid, distilled water, acetone, ethanol, distilled water and finally allowed to air dry to remove the negligible amount of surface residues. All solvents and chemicals were of analytical grade and were used without further purification.

Deposition of TiO_2 thin films

The procedure for preparing of TiO_2, TiO_2/Al_2O_3 thin films by CBD method consists of three main steps, including the solution preparation, formation of thin films and annealing the films, TTIP (0.2M) was dissolved in Ethanol C_2H_5OH (40 ml) and isopropanol (10 ml) to constitute a solution (A). Solution (A) was then magnetically stirred at room temperature for 10 min for homogeneity, using a water bath to start the formation of TiO_2 nanoparticles. The pH of the solution was adjusted at 5. Two ITO coated glass used as substrates which were immersed into the solution (A) for 1 h at room temperature. Thin films of TiO_2 material were deposited onto glass plates, then dried in air for 24 h. One of these as-prepared film was annealed at 500 °C.

Deposition of TiO_2/Al_2O_3 thin films

$AlCl_3 \cdot 6H_2O$ (0.05M) was dissolved in ethanol (10 ml) and the stirred for 2 h, constituting a solution (B) Then, the both solutions (A) (freshly prepared) and (B) were thoroughly mixed together under magnetic stirring for 1 h at 40 °C. After room temperature cooling, ITO coated glass substrates were immersed into the resulting solution with adjusted pH 4.2 for 1 h at room temperature. The deposited films were then dried in air for 24 h. Similarly, one of them was annealed at 500 °C. High-quality and highly transparent TiO_2/Al_2O_3 nanostructured thin films were obtained and subjected for further characterizations.

Characterization techniques

The deposited TiO_2 thin films were characterized for their structural, morphological, and compositional properties. The crystal structure and crystallographic data were obtained from X-ray diffractometer (XRD) (Ultima IV of Rigaku Corporation, Japan) with CuK_α ($\lambda = 1.54056$ Å).

Fourier transform-infrared (FT-IR) spectra (FT-IR JASCO-4600) were scanned from 4000 to 400 cm^{-1} using the transmittance mode.

Raman spectra were recorded on a Jobin Yvon Horibra LABRAM-HR instrument within a range of 200–1800 cm^{-1} by a scanning resolution of 1 cm^{-1}, applying a back scattering geometry.

The surface morphology of TiO_2 and TiO_2/Al_2O_3 films were investigated by a Field emission-scanning electron microscope (FE-SEM) using FESEM-JEOL JEM-6360 Mira-3, Tascan, Republic of Czech.

Values of absorption coefficient (α) and band-gap energy (E_a) were calculated from the data obtained from UV-visible absorption spectra measured using a U-V Double Beam Spectrophotometer V-750 (Jasco Corp., Tokyo, Japan) at wavelengths scanned in the range of 250–700 nm.

Results and discussion

Structure Analysis

The XRD patterns of TiO_2 and TiO_2/Al_2O_3 thin films deposited on the ITO coated glass substrate using the CBD method were presented in Fig. 1. The crystal structure and phase of the deposited TiO_2 thin films before annealing (Fig. 1, *a*) are predominantly anatase and rutile as clearly evidenced by the appearance of the following sublattice peaks: 25.28°, 37.80°, 48.06°, 53.92°, 55.08°, 62.72°, 68.80°, 70.32° and 75.10° which were in-

dexed consequently as (101) A, (004) A, (200) A, (106) A, (211) R, (116) A, (301) R, (107) A, (216) A, where A for anatase phase and R for rutile phase [31], [32]. However, after addition of $AlCl_3 \cdot 6H_2O$, the XRD pattern of TiO_2/Al_2O_3 thin film before annealing (Fig. 1, *b*) shows additional three broad sublattice peaks within the diffraction angle range 20° and 80°. Where no obvious crystalline phase, indicating that this thin film is present in a defect crystal structure (amorphous-like) [33]. After annealing at 500 °C for 2 h, the XRD pattern of TiO_2 thin film (Fig. 1, *c*) exhibits sublattice peaks at 25.28°, 37.88°, 48.02°, 54°, 55.06°, 62.18°, 62.78° and 75.16°, indexed as (101), (004), (200), (105), (211), (204), and (215), respectively, which are clearly indicative for the existence of a tetragonal anatase symmetry [34]. It is also clear that no other peaks for brookite or rutile phases were appeared, suggesting the high purity of annealed TiO_2 thin film. These results were agreed well with JCPDS card number 21-1272. The most intense reflection corresponding to the (101) plane, whose intensity decreases with addition of $AlCl_3 \cdot 6H_2O$) (Fig. 1, *c*), also indicates the presence of the only anatase phase for the TiO_2/Al_2O_3 film [35]. The estimated lattice parameters were found to be $a = b = 0.3785$ nm and $c = 0.9513$ nm. The average crystallite size was computed using the Debye-Scherrer's equation:

$$D = \frac{K\lambda}{\beta \sin\theta}, \tag{1}$$

where D is the average crystallite size, K is the Debye Scherrer's constant ($K = 0.94$), λ is the wavelength of the $CuK_{\alpha\text{-radiation}}$ ($\lambda = 1.5406$ Å), β is the full width half maximum (FWHM) of the peak, and θ is the Bragg's angle [36]. The average crystallite size (D) for TiO_2 was found to be 58.6 and 22.8 nm before and after annealing, respectively. Whereas that for TiO_2/Al_2O_3 is 56 nm before annealing, which then decreases to 17 nm when the film annealed at 500 °C, indicating an improved crystallinity upon annealing. Moreover, the average of spacing between the diffracted planes was calculated by the Bragg law:

$$d = \frac{n\lambda}{2 \sin\theta}, \tag{2}$$

where d is the average of spacing between diffracting planes, and found to be 2.99 nm and thereafter remarkably reduces to 2.38 nm for annealed film at 500 °C.

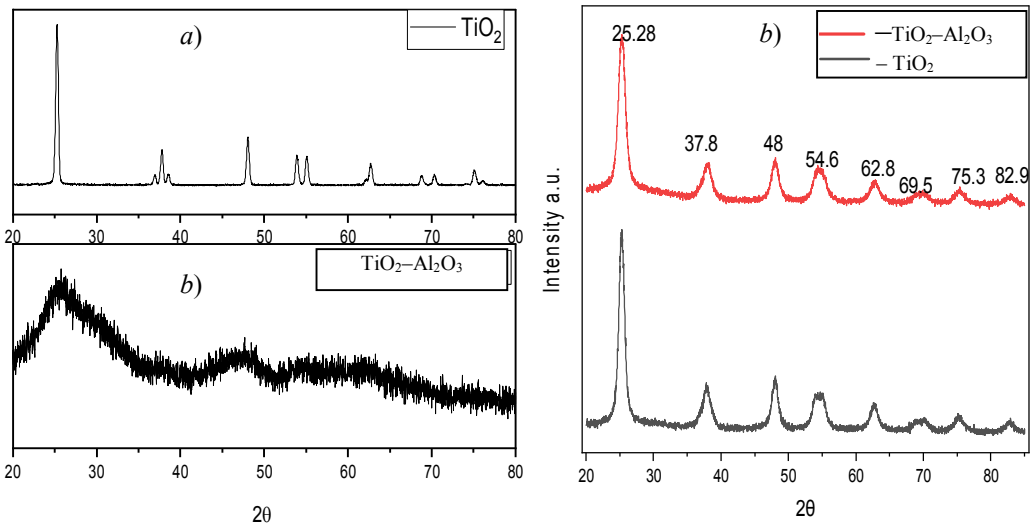

Fig. 1. XRD patterns of (*a*) TiO_2, (*b*) TiO_2/Al_2O_3 before annealing and (*c*) annealed TiO_2 and TiO_2/Al_2O_3 at 500 °C

Fourier transform-infrared (FT-IR) analysis

FT-IR spectroscopy can be successfully applied to study the formation of as-prepared nanocrystalline sized oxides and characterize the surface state of deposited nanoparticles by CBD. FT-IR results complements the information obtained from XRD analysis. It represents the integration of all data that is used to understand and refine the structure of films more efficiently [37]–[39]. The obtained absorption peak frequencies indicate the type of functional group present in the material.

Figure 2 depicts many absorption bands within wide ranges of 450–1000 cm^{-1}, and 3400–4000 cm^{-1}, while no apparent bands found in the range of 1000–3400 cm^{-1}. In the first range, there are many sharp peaks can be attributed to characteristic to Ti–O and Ti–O–Ti stretching and bending vibrational modes for rutile TiO_2 [40], whereas the absorption band appeared at 1400 cm^{-1} is attributed to C–H bonds of $–CH_3$ group [41] These bands become sharper by addition of $AlCl_3$, particularly in the region 3400–4000 cm^{-1} assigned to the stretching O–H bond [42], [43].

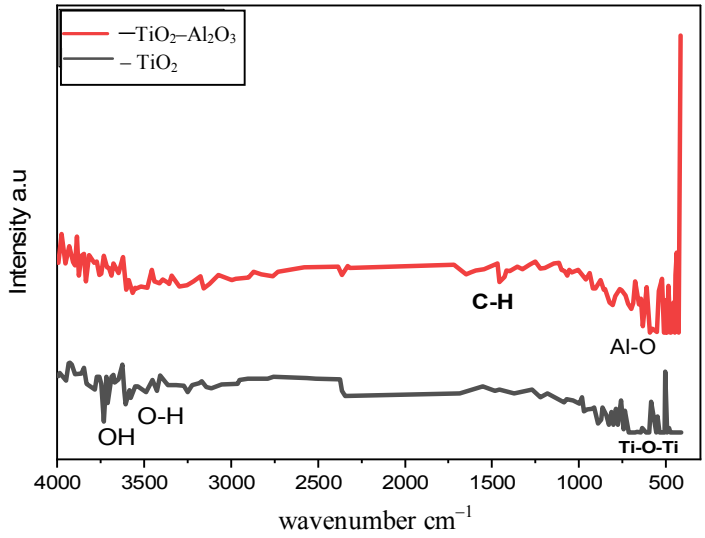

Fig. 2. FT-IR spectra of TiO_2 and TiO_2–Al_2O_3 before annealing

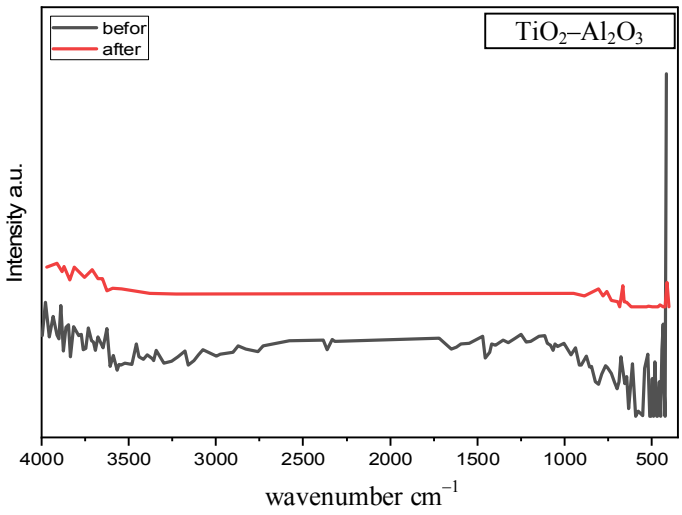

Fig. 3. FT-IR spectra of TiO_2/Al_2O_3 before and after annealing

The FT-IR spectrum of the annealed TiO_2 thin film at 500 °C is shown in Fig. 3, the strong bands located around 460–640 cm^{-1} are associated with the Ti–O–Ti stretching vibration, indicating the formation of TiO_2 anatase phase [44]–[46]. There is a clear shifting in the band around 3640–3870 cm^{-1} due to the O–H stretching vibration. However, the band due to the Al–O stretching vibrations of the octahedral coordinated Al site can be seen in the range of 500–880 cm^{-1} [47]–[49].

Raman Spectroscopy

Raman shifts are affected by the vibration of the electronic polarization of components in the films, which depend on bonding properties such as atomic distance and bonding angle for the product structure changed when the chemical bond was rearranged. According to the data of Raman spectroscopy, anatase phase was formed mostly in the film at 140, 386, 504, and 627 cm^{-1}, and it is clearly evidenced by the appearance of an anatase peak at 144 cm^{-1} as shown in Fig. 4. This peak is well known as a probe, and is very sensitive to the anatase phase in TiO_2 films [50], [51]. A large distortion of the curve occurs by the addition of Al_2Cl_3, indicating a change in the composition of the sample. A new and wide peak for the aluminum and titanium phases is also observed. After annealing many peaks of TiO_2 are observed in the ring of 0–1000 cm^{-1} (Fig. 5) with a sharp peak assigned to anatase phase. Figure 6 present Raman spectra of TiO_2/Al_2O_3 before and after annealing. Sharp and clear peaks shown after annealing the film are clear evidence for the improvement of the crystal structure of the films upon annealing.

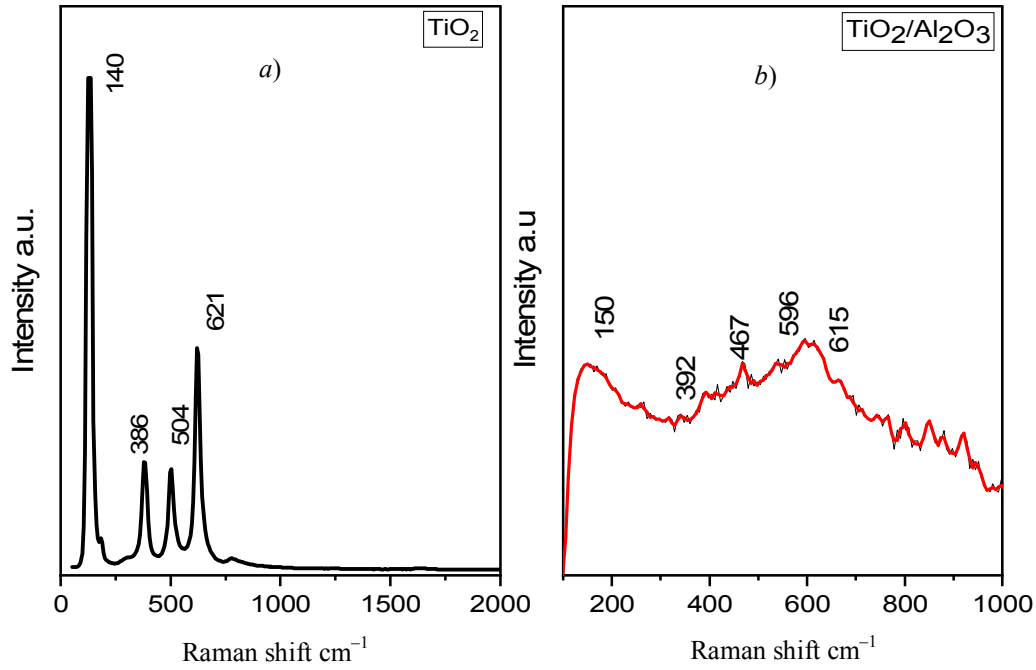

Fig. 4. Raman spectra of (*a*) TiO_2, and (*b*) TiO_2–Al_2O_3 before annealing

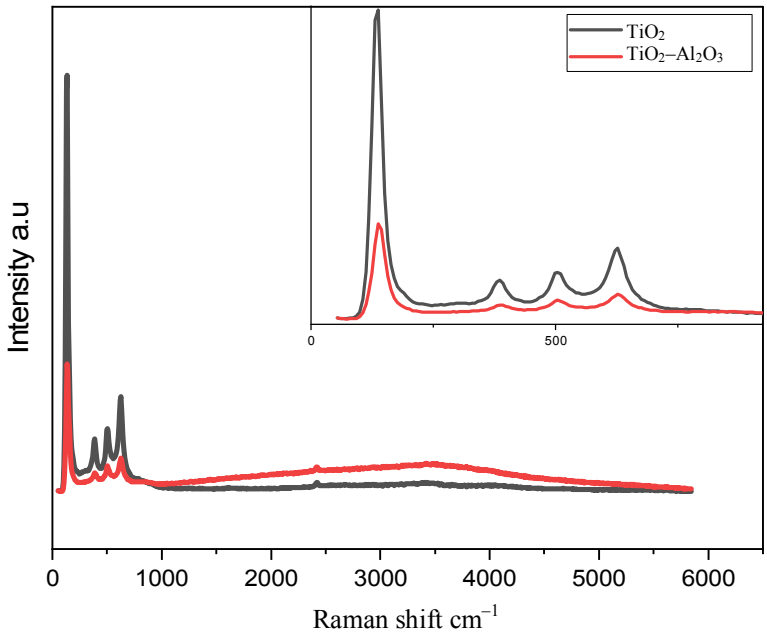

Fig. 5. Raman spectra of TiO_2 and TiO_2/Al_2O_3 after annealing at 500 °C

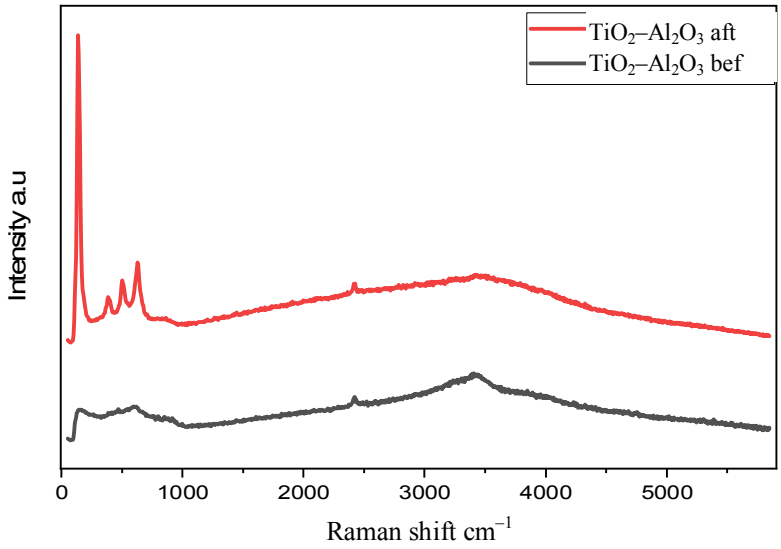

Fig. 6. Raman spectra of TiO_2/Al_2O_3 before and after annealing

Field emission-scanning electron microscopy (FE-SEM)

SEM analysis is a powerful tool for examining and characterizing nanoparticles, fracture surfaces, surface morphologies, constituents and microstructures of prepared materials. Figure 7, *a* shows spherical, uniform sized TiO_2 nanoparticles which seem to be completely covering the ITO glass substrate [52]. Due to the larger surface-to-volume ratio, the surface activity of the film without doubt results in a higher degree of UV light absorption. While, an irregular shaped nanoparticles of the TiO_2/Al_2O_3 are clearly observed in Fig. 7, *b* without significantly homogenous distribution [53], which are entirely changed to nanosheets.

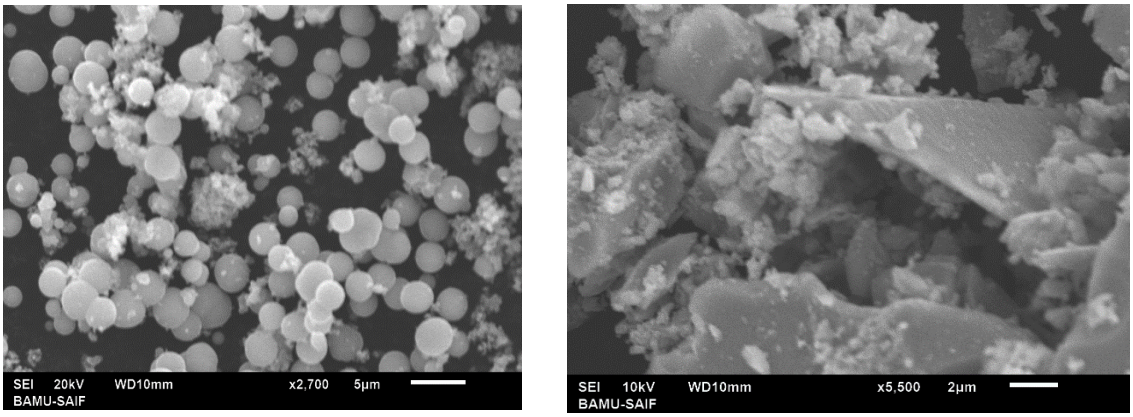

a) *b*)

Fig. 7. FE-SEM images of (*a*) TiO_2, and (*b*) TiO_2/Al_2O_3 thin films

Optical studies

Figure 8, *a* shows the optical absorption spectra of as-prepared and annealed TiO_2 thin films in the wavelength range of 300–500 nm. Distinct strong absorption peaks are seen in the range of 310 to 340 nm, which is due to the excitation of electrons from the valence band to the conduction band of TiO_2 under influence of light absorption. It can be observed that the absorption edge of annealed TiO_2 slightly shifts to 350 nm (i. e., red shift), which can be attributed to grain size effects on thermal treatment.

On other hand, the absorption edge is found to shift to the visible region with addition of Al_2O_3 as shown in Fig. 8, *b*. This implies that the presence of Al_2O_3 can enhance the photocatalytic activity of TiO_2 under visible-light excitation. Further, after annealing TiO_2/Al_2O_3 thin film, the absorption edge shifts to a longer wavelength with the increased intensity [43], [54]. The absorbance data was also used to calculate the direct band-gap energy of the TiO_2 thin film by equation (3):

$$a = \frac{A(hv - E_g)^n}{hv}. \tag{3}$$

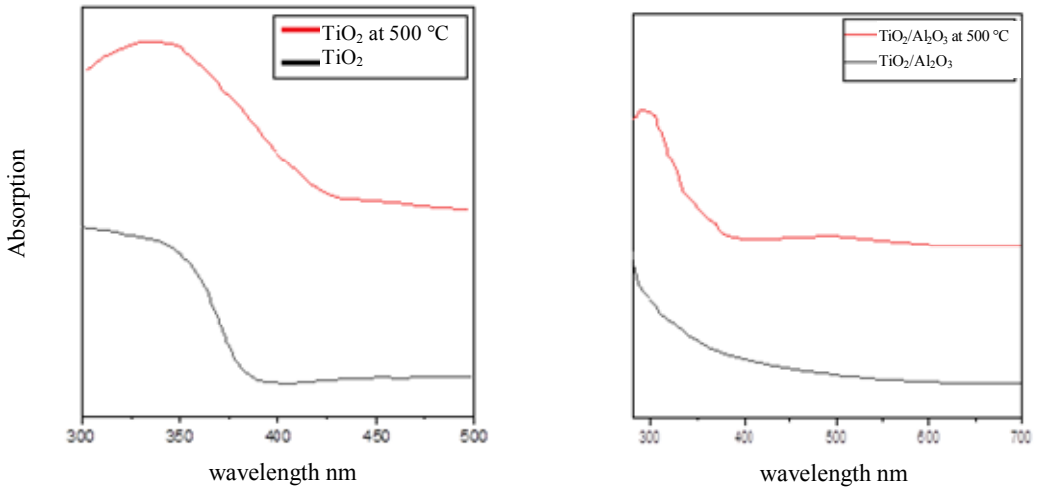

a) *b*)

Fig. 8. Optical absorption spectra of TiO_2 (*a*) and TiO_2/Al_2O_3 (*b*) films before and after annealing

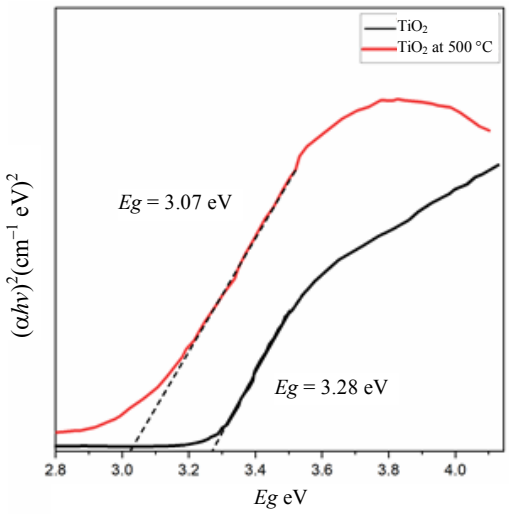

Fig. 9. Determination of band-gap energy of TiO_2 before and after annealing

Figure 9 illustrates plots of $(\alpha h\nu)^2$ *vs.* $h\nu$ for the as-deposited and annealed TiO_2 thin films, which are linear at the absorption edge, confirming a direct band-gap material. Values of the direct band-gap energy of the as-deposited and annealed TiO_2 thin films are determined by extrapolating the linear portion of the curve. The optical band-gap energy of as-deposited TiO_2 thin film is found to be 3.28 eV, which is slightly greater than that of the annealed TiO_2 thin film (3.07 eV). Because of the slight improvement in the crystallization after annealing, the absorbance edge showed red shift to some extent.

However, the value of E_g for TiO_2/Al_2O_3 thin film was estimated as 3.32 eV, that means it slightly increases on adding Al_2O_3, and similarly decreases upto 3.14 eV after annealed at 500 °C, due to the improved crystallization [55], [56], as shown in Fig. 10.

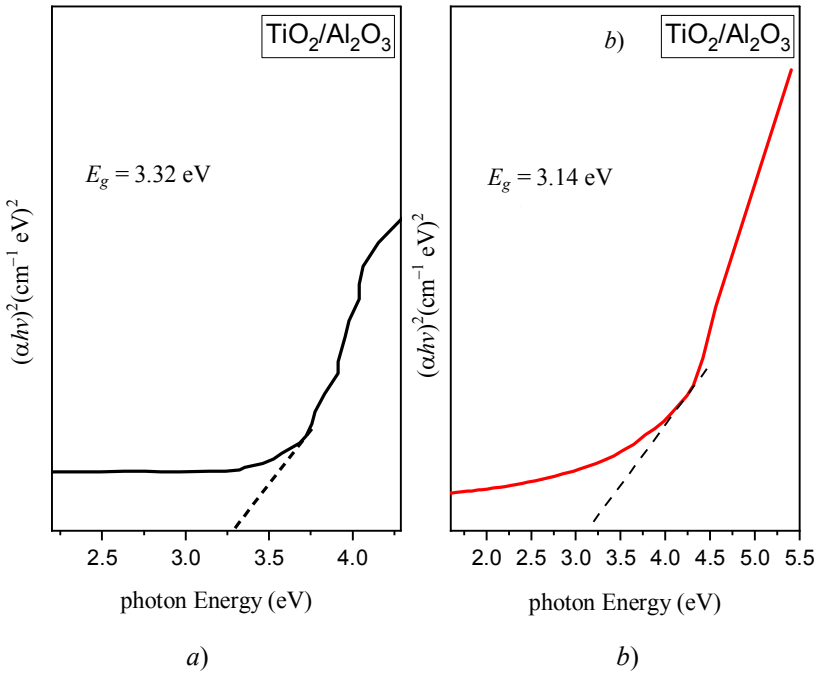

Fig. 10. Determination of band-gap energy of TiO_2/Al_2O_3 before (*a*) and after annealing (*b*)

Conclusion

Despite of its simplicity and low cost, CBD was proven to be an effective and successful technique in depositing and preparing thin films of metals oxides. In the present work, CBD was successfully utilized for preparation of TiO_2 and TiO_2/Al_2O_3 thin films deposited on ITO glass substrates. The combined XRD and FE-SEM results revealed a spherical structure of anatase phase for TiO_2 film and a tetragonal anatase structure for TiO_2/Al_2O_3 film, and that the grain size goes on decreasing when doped with Al_2O_3 and annealed at 500 °C for 2 h. Interestingly, the spherically shaped nanoparticles of TiO_2 turned to nanosheets after Al_2O_3 addition. However, FT-IR and Raman results confirmed the structures of prepared thin films and explore the advantages of annealing and Al_2O_3 addition in the enhancement of crystallinity. The optical band-gap energy of TiO_2 thin film was found to be 3.28 eV, which then slightly decreased upto 3.07 eV after annealing. For TiO_2/Al_2O_3 thin film, E_g was reduced from 3.32 to 3.14 eV after annealed. Generally, the structural, morphological and optical properties investigated in this study confer the deposited TiO_2 and TiO_2/Al_2O_3 thin films promising, near future applications in electronic and optical devices.

References

1. Fabrication of multifunctional coating which combines low-e property and visible-light-responsive photocatalytic activity / M. Okada [et al.] // Thin Solid Films. – 2003. – Vol. 442. – P. 217–221.
2. TiO_2 and TiO_2–SiO_2 thin films and powders by one-step soft-solution method: Synthesis and characterizations / A. Ennaoui [et al.] // Sol. Energy Mater. Sol. Cells. – 2006. – Vol. 90. – P. 1533.
3. Weinberger, R. Titanium dioxide photocatalysts produced by reactive magnetron sputtering / R. Weinberger, R. B. Garber // Appl. Phys. Lett. – 1995. – Vol. 66. – P. 2409.
4. Titanium oxide thin films for NH_3NH_3 monitoring: Structural and physical characterizations / D. Manno [et al.] // J. Appl. Phys. – 1997. – Vol. 82. – P. 54.
5. Wang, Z. Fabrication and electrochromic properties of spin-coated TiO_2 thin films from peroxo-polytitanic acid / Z. Wang, X. Hu // Thin Solid Films. – 1999. – Vol. 352. – P. 62–65.
6. Liu, J. X. Sol-gel deposited TiO_2 film on NiTi surgical alloy for biocompatibility improvement / J. X. Liu [et al.] // Thin Solid Films. – 2003. – Vol. 429. – P. 225–230.
7. Optical and structural properties of TiO_2 thin films prepared by sol-gel spin coating / A. Elfanaoui [et al.] // International journal of hydrogen energy. – 2011. – Vol. 36. – P. 4130–4133.
8. Bendavid, A. Deposition and modification of titanium dioxide thin films by filtered arc deposition / A. Bendavid, P. J. Martin, H. Takikawa // Thin Solid Films. – 2000. – Vol. 360. – P. 241–249.
9. Williams, L. M. Structural properties of titanium dioxide films deposited in an rf glow discharge / L. M. Williams, D.W. Hess, J. Vac // Sci. Technol. A. – 1983. – Vol. 1. – P. 1810.
10. Elaboration and characterization of titania coatings / S. B. Amor [et al.] // Thin Solid Films. – 1997. – Vol. 293. – P. 163–169.
11. Preparation of Rutile TiO_2 Films by RF Magnetron Sputtering, Jpn. / K. Okimura [et al.] // J. Appl. Phys. – 1995. – Vol. 34. – P. 4950.

12. Gilo, M. Properties of TiO_2 films prepared by ion-assisted deposition using a gridless end -Hall ion source / M. Gilo, N. Croitoru // Thin Solid Films. – 1996. – Vol. 283. – P. 84–89.
13. Determination of optical constants of solgel-derived inhomogeneous TiO_2 thin films by spectroscopic ellipsometry and transmission spectroscopy / M. Mosaddeq-ur-Rahman [et al.] // Appl. Opt. – 1998. – Vol. 37. – P. 691–697.
14. Suzuk, S. Optical gain and crystal symmetry in III–V nitride lasers / S. Suzuk, I. Ohsak, N. Ando // Jpn. J. Appl. Phys. – 1996. – Vol. 35. – P. 1862.
15. The synthesis of TiO_2 thin film by Chemical Bath Deposition (CBD) method / A. ElFanaoui [et al.] // Ann. Chim. Sci. Mat. – 2011. – Vol. 36. – P. 37.
16. Mohan, S. A review of ion beam assisted deposition of optical thin films / S. Mohan, M. Krishna // Bergamon. – 1994. – Vol. 46. – P. 645–659.
17. Characteristics of titanium oxide films deposited by an activated reactive evaporation method / T. Fujii [et al.] // J. Mater. Res. – 1994. – Vol. 9. – P. 1468–1473.
18. Effect of Annealing Temperature on the Photocatalytic Activity of TiO_2 Thin Films / C.-P. Lin [et al.] // Energy Procedia. – 2013. – Vol. 34. – P. 627–636.
19. Impact of annealing temperature on structural, morphological and optical properties of GO–TiO_2 thin films prepared by spin coating technique / A. Timoumi [et al.] // Super lattices and Microstructures. – 2020. – Vol. 139. – P. 106423.
20. Singh, J. Thermal annealing induced evolution of morphological, structural, optical and photocatalytic properties of Ag–TiO_2 nanocomposite thin films / J. Singh, K. Sahu, S. Mohapatra // Journal of Physics and Chemistry of Solids. – 2019. – Vol. 129. – P. 317–323.
21. Paul, T. C. Optical constants and dispersion energy parameters of Zn-doped TiO_2 thin films prepared by spray pyrolysis technique / T. C. Paul, J. Podder, M. H. Babu // Surfaces and Interfaces. – 2020. – Vol. 21. – P. 100725.
22. Lide, D. R. CRC PR Inc. / D. R. Lide // CRC Handbook of Chemistry and Physics. – 2008. – Vol. 89.
23. HfO_2HfO_2 and $Al_2O_3Al_2O_3$ gate dielectrics on GaAs grown by atomic layer deposition / M. M. Frank [et al.] // Appl. Phys. Lett. – 2005. – Vol. 86.
24. Low-Temperature Al_2O_3 Atomic Layer Deposition / M. Groner [et al.] // Chem. Mater. – 2004. – Vol. 16. – P. 639–645.
25. Maruyama, T. Aluminum oxide thin films prepared by chemical vapor deposition from aluminum acetylacetonate / T. Maruyama, S. Arai // Appl. Phys. Lett. – 1992. – Vol. 60. – P. 322–323.
26. A. High-k Gate Dielectrics for Emerging Flexible and Stretchable Electronics / B. Wang [et al.] // Chem. Rev. – 2018. – Vol. 118. – P. 5690–5754.
27. Aguilar-Frutis, M. Optical and electrical properties of aluminum oxide films deposited by spray pyrolysis / M. Aguilar-Frutis, M. Garcia, C. Falcony // Appl. Phys. Lett. – 1998. – Vol. 72. – P. 1700–1702.
28. Deposition of alumina thin film by dual magnetron sputtering: Is it γ-Al_2O_3 / W. Engelhart [et al.] // J. Acta Mater. – 2011. – Vol. 59. – P. 7757–7767.
29. Eco-friendly synthesis of cynomorium coccineum extract for controlled production of copper nanoparticles for sorption of methylene blue dye / N. Sebeia [et al.] // Arab. J. Chem. – 2020. – Vol. 13. – P. 4263–4274.

30. K. Kefeni, Evaluation of charcoal ash nanoparticles pollutant removal capacity from acid mine drainage rich in iron and sulfate / K. Kefeni, B. Mamba // J. Clean. Prod. – 2020. – Vol. 251. – P. 119–128.

31. Zhitomirsky, I. Electrolytic TiO_2–RuO_2 deposits / I. Zhitomirsky // J. Mater. Sci. – 1999. – Vol. 34. – P. 2441–2447.

32. Cathodic electrodeposition of amorphous titanium oxide films from an alkaline solution bath / C. D. Lokhande [et al.] // J. Mater. Sci. – 2004. – Vol. 39. – P. 6606–6610.

33. Synthesis and characterization of amorphous Al_2O_3 and γ-Al_2O_3 by spray pyrolysis / Z. Wang [et al.] // Green Process Synth. – 2016. – Vol. 5. – P. 305–310.

34. Green Synthesis of TiO_2 Nanoparticles Using Aloe Vera Extract / K. Ganapathi [et al.] // International Journal of Advanced Research in Physical Science. – 2015. – Vol. 2. – P. 28–34.

35. Tribocorrosion behavior of TiO_2/Al_2O_3 nanolaminate, Al_2O_3, and TiO_2 thin films produced by atomic layer deposition / P. Alves [et al.] // Repositorio Institucional Unesp. – 2018. – P. 1077–1082.

36. Nanostructured TiO_2 Thin Films by Chemical Bath Deposition Method for High Photo Electrochemical Performance / S. V. Kite [et al.] // Materials Research Express. – 2018.

37. Optical and structural properties of aluminium oxide thin films prepared by a non-aqueous sol-gel technique / N. Avci [et al.] // J. Sol-Gel Sci Technol. – 2011. – Vol. 59. – P. 327–333.

38. Optical investigations and optical constant of nano lithium niobate deposited by spray pyrolysis technique with injection of Li_2CO_3 and Nb_2O_5 as raw materials / M. A. Fakhri [et al.] // Journal of Materials Science: Materials in Electronics. – 2018. – Vol. 29. – P. 9200–9208.

39. Optical properties of micro and nano $LiNbO_3$ thin film prepared by spin coating / M. A. Fakhri [et al.] // Optics Laser Technology. – 2018. – Vol. 103. – P. 226–232.

40. Naayi, S. A. FTIR and X-ray diffraction analysis of Al_2O_3 nanostructured thin film prepared at low temperature using Spray pyrolysis method / S. A. Naayi, A. I. Hassan, E. T. Salim // International Journal of Nano electronics and Materials. – 2022. – Vol. 11. – P. 1–6.

41. Govindasamy, G. Investigations on the synthesis, optical and electrical properties of TiO_2 thin films by chemical bath deposition (CBD) method / G. Govindasamy, P. Murugasen, S. Sagadevan // Mat. Res. – 2016. – Vol. 19. – P. 413–419.

42. TiO_2 thin films studied by FTIR, AFM and spectroscopic ellipsometry / Y. Bouachiba [et al.] // Int. J. Nanoparticles. – 2013. – Vol. 6. – P. 169–177.

43. Adamczyk, A. The FTIR studies of gels and thin films of Al_2O_3–TiO_2 and Al_2O_3–TiO_2––SiO_2 systems / A. Adamczyk, E. Długon // Spectrochimica Acta A. – 2012. – Vol. 89. – P. 11–17.

44. Characterisation of stoichiometric sol-gel mullite by fourier transform infrared spectroscopy Int / P. Padmaja [et al.] // J. Inorg. Mater. – 2001. – Vol. 3.

45. Ali, A. M. Effect of hydrogen dilution on the growth of nanocrystal line silicon films at high temperature by using plasma-enhanced chemical vapor deposition / A. M. Ali, S. Hasegawa // Thin Solid Film. – 2003. – Vol. 43. – P. 68–73.

46. Transformation of rutile to TiO_2-II in a high pressure hydrothermal environment / K. Spektor [et al.] // J. Solid State Chem. – 2013. – Vol. 206. – P. 209–216.

47. Influence of Al_2O_3 Template and Process Parameters on Atomic Layer Deposition and Properties of Thin Films Containing High-Density TiO_2 Phases / K. Möls [et al.] // Coatings. – 2021. – Vol. 11.
48. Nanosized Al_2O_3–TiO_2 oxide powder with enhanced porosity obtained by sol-gel method / T. Dascalescu [et al.] // Rev. Roum. Chim. – 2014. – Vol. 59. – P. 125–134.
49. Effect of TiO_2 nanostructures on specific capacitance of Al_2O_3–TiO_2 composite film on etched aluminum foil formed by the sol-gel and anodizing / J. Liun [et al.] // Ceramics International. – 2014. – Vol. 40. – P. 3687–3692.
50. Structural study of TiO_2 thin films by micro-Raman spectroscopy / A. Niilisk [et al.] // Central European Science Journals. – 2006. – Vol. 4. – P. 105–116.
51. Database of slandered Raman spectra of Minerals and Related Inorganic crystals / A. Wang [et al.] // Applied Spectrascopy. – Vol. 48, № 8. – P. 959–968.
52. Dhanapandian, S. Effect of deposition parameters on the properties of TiO_2 thin films prepared by spray pyrolysis / S. Dhanapandian, A. Arunachalam, C. Manoharan // J. Sol-Gel Sci. Technol. – 2016. – Vol. 77. – P. 119–135.
53. Ali1, A. S. Hydrothermal synthesis of TiO_2/Al_2O_3 nanocomposite and its application as improved sonocatalyst / A. S. Ali1, A. J. Mohammed, H. R. Saud // International Journal of Engineering &Technology. – 2018. – Vol. 7. – P. 22–25.
54. Characteristics modification of TiO_2 thin films by doping with silica and alumina for self-cleaning Application / D. M. Chien [et al.] // Journal of Experimental Nanoscience. – 2009. – Vol. 4. – P. 221–232.
55. Photosensitive nanostructured TiO_2 grown at room temperature by novel “bottom-up” approached CBD method / U. M. PatilS [et al.] // Journal of Alloys and Compounds. – 2011. – Vol. 509. – P. 6196–6199.
56. Arıer, U. O. Influence of Al_2O_3 : TiO_2 ratio on the structural and optical properties of TiO_2–Al_2O_3 nano-composite films produced by sol gel method / U. O. Arıer, F. Z. Tepehan // Composites B. – 2014. – Vol. 58. – P. 147–151.

Получено 18.08.2022